

Title	Broadband optical equalizer using fault-tolerant digital micromirrors
Authors	Riza, Nabeel A.;Mughal, M. Junaid
Publication date	2003-06-30
Original Citation	Riza, N. A. and Mughal, M. J. (2003) 'Broadband optical equalizer using fault-tolerant digital micromirrors'. Optics Express, 11 (1313), pp. 1559-1565. doi: 10.1364/OE.11.001559
Type of publication	Article (peer-reviewed)
Link to publisher's version	https://www.osapublishing.org/oe/abstract.cfm?uri=oe-11-13-1559 - 10.1364/OE.11.001559
Rights	© 2003 Optical Society of America
Download date	2025-05-21 05:58:22
Item downloaded from	https://hdl.handle.net/10468/10250

Broadband optical equalizer using fault-tolerant digital micromirrors

Nabeel A. Riza and M. Junaid Mughal

Nuonics, Inc., 3361 Rouse Road, Suite 170, Orlando, FL 32817
nabeel@nuonics.com

Abstract: For the first time, the design and demonstration of a near continuous spectral processing mode broadband equalizer is described using the earlier proposed macro-pixel spatial approach for multi-wavelength fiber-optic attenuation in combination with a high spectral resolution broadband transmissive volume Bragg grating. The demonstrated design features low loss and low polarization dependent loss with broadband operation. Such an analog mode spectral processor can impact optical applications ranging from test and instrumentation to dynamic all-optical networks.

© 2003 Optical Society of America

OCIS codes: (120.2440) Filters, (060.2310) Fiber optics, (230.6120) Spatial Light Modulators

References and links

1. S. H. Huang, X. Y. Zou, S.-M. Hwang, A. E. Willner, Z. Bao, and D. A. Smith, "Experimental demonstration of dynamic network equalization of three 2.5 Gb/s WDM channels over 100 km using acousto-optic tunable filters," *IEEE Photon. Technol. Lett.* **8**, 1243-1245 (1996).
2. H. S. Kim, S. H. Yun, H. K. Kim, N. Park, and B. Y. Kim, "Actively gain-flattened erbium-doped fiber amplifier over 35 nm by using all fiber acousto-optic tunable filters," *IEEE Photon. Technol. Lett.* **10**, 790-792 (1998).
3. J. Sapriel, D. Charissoux, V. Voloshinov, V. Molchanov, "Tunable acoustooptic filters and equalizers for WDM applications," *IEEE J. Lightwave Technol.* **20**, 892-899 (2002).
4. M. C. Parker, A. D. Cohen, R. J. Mears, "Dynamic digital holographic wavelength filtering," *IEEE J. Lightwave Technol.* **16**, 1259-1270, (1998).
5. J. P. Kondis, B. A. Scott, A. R. Ranalli, R. Lindquist, "Liquid crystals in bulk optics-based DWDM optical switches and spectral equalizers," *IEEE LEOS 14th Ann. Mtg. Proc.* **1**, 292-293 (2001).
6. K. Hirabayashi, M. Wada, C. Amano, "Optical-fiber variable-attenuator arrays using polymer-network liquid crystal," *IEEE Photon. Technol. Lett.* **13**, 487-489 (2001).
7. J. E. Ford and J. A. Walker, "Dynamic spectral power equalization using micro-opto-mechanics," *IEEE Photon. Technol. Lett.* **10**, 1440-1442, (1998).
8. Liaw Shien-Kuei, Ho Keang-Po, Chi Sien, "Dynamic power-equalized EDFA module based on strain tunable fiber Bragg gratings," *IEEE Photon. Technol. Lett.* **11**, 797-799, (1999).
9. P.M.J Schiffer, C.R Doerr, L. W. Stulz, M. A. Cappuzzo, E. J. Laskowski, A. Paunescu, L.T. Gomez, "Smart dynamic wavelength equalizer with on-chip spectrum analyzer," *IEEE Photon. Technol. Lett.* **12**, 1019-1021, (2000).
10. S. Wada, S. Abe, Y. Ota, B. Reichman, T. Imura, C. A. Daza, "Variable gain equalizer using magneto-optics," *Optical Fiber Communication Conference (OFC)*, 324-326, (2002).
11. N. A. Riza and Sarun Sumriddetchkajorn, "Digitally controlled fault tolerant multiwavelength programmable fiber-optic attenuator using a two dimensional digital micromirror devices," *Optics Letters*, **24**(5), 282-284 (1999).
12. N. A. Riza and N. Madamopoulos, "Synchronous amplitude and time control for an optimum dynamic range variable photonic delay line," *Appl. Opt.* **38**, 2309-2318 (1999).
13. N. A. Riza, "Fault-tolerant fiber-optical beam control modules," US Patent No. 6,222,954, April 24, 2001.
14. N. A. Riza, "Multi-technology multi-beam-former platform for robust fiber-optical beam control modules," US Patent No. 6,525,863, Feb. 25, 2003.
15. N. A. Riza and N. Madamopoulos, "High Signal-to-Noise Ratio Birefringence Compensated Optical Delay Line using a Noise Reduction Scheme," *Opt. Lett.* **20**, 2351-2353, (1995).
16. Z. Yaqoob, Azhar A. Rizvi and N. A. Riza, "Free-space wavelength multiplexed optical scanner," *Appl. Opt.* **40**, 6425-6438, (2001).

1. Introduction

The ability to actively control the power in the individual spectral components of a signal have long been recognized as a powerful signal processing operation benefiting fields such as audio systems, microwave radar, and more recently fiber-optic communications. The signal processor that implements this spectral processing is commonly called an equalizer or spectral filter. Various technologies have been proposed and implemented to realize all-optical equalizers for the wavelength division multiplexed (WDM) optical communications arena. Some of the efforts reported in the published literature include the use of acousto-optics [1-3], liquid crystals [4-6], microelectromechanical systems (MEMS) mirrors [7], tunable fiber Bragg gratings [8], thermo-optics [9], and magneto-optics [10]. Earlier we proposed a fault-tolerant robust mechanism for fiber-optical attenuation control involving macro-pixel beam spoiling coupled with fiber-optics and spatially independent wavelength processing [11-14]. A main feature of this approach versus single pixel or single optical control site approaches is that many pixels across a particular beam spatial zone provide a multi-dimensional gain control mechanism leading to hardware redundancy and hence fault-tolerance, in addition to faster and higher precision gain controls when using moving parts MEMS pixels. As suggested earlier, pixels within the macro-pixel can operate in either pure phase-only mode or an amplitude reduction mode to enable the required beam spoiling to generate the free space-to-fiber beam coupling loss to produce the wanted attenuation. Our earlier work demonstrated an infrared band (i.e., 1550 nm center wavelength) MEMS optical equalizer using a visible band design tilt-mode micromirror macro-pixel coupled with a discrete-mode fiber connectorized wavelength dispersive optic. There are spectral processing applications such as test and measurement and photonic signal processing where hardware discretization of wavelength is not preferred and where near continuous analog-mode high resolution spectral control is desired across a broad optical spectrum. With this motivation in mind, the present letter describes an equalizer using an optimized infrared band macropixel MEMS device coupled with a non-discretized wavelength dispersive optic to realize the desired powerful analog spectral processor module. Specifically, the experiments show that indeed a high dynamic range, all-digital control and hence fully repeatable, broadband, low loss, high attenuation and wavelength resolution equalizer can be realized using the earlier proposed macro-pixel based fault-tolerant equalizer design.

2. Equalizer design

Figures 1(a) and (b) show the designed equalizer structure top and side views, respectively. Light enters via a single mode fiber (SMF) coupled to an optical circulator C that directs the input light to a fiber graded-index (GRIN) lens FL that acts as a beam collimator. At the minimum beam waist radius w_i location of the Gaussian beam from the fiber lens, a transmissive volume Bragg grating G is placed as an analog-mode spatial wavelength multiplexing optic. The distance between the fiber lens and grating is L. The incident Gaussian beam on the grating is Bragg matched for a given λ_c central wavelength for the spectral processor with the incident beam Bragg angle θ_c given by $\sin \theta_c = (\lambda_c / 2l)$, where l is the grating period. The grating G diffracts light in the first order centered around the Bragg angle with an angular spread given by $2\Delta\theta = \theta_{\max} - \theta_{\min}$, where the angle θ is measured from the grating normal. Using the classic grating equation,

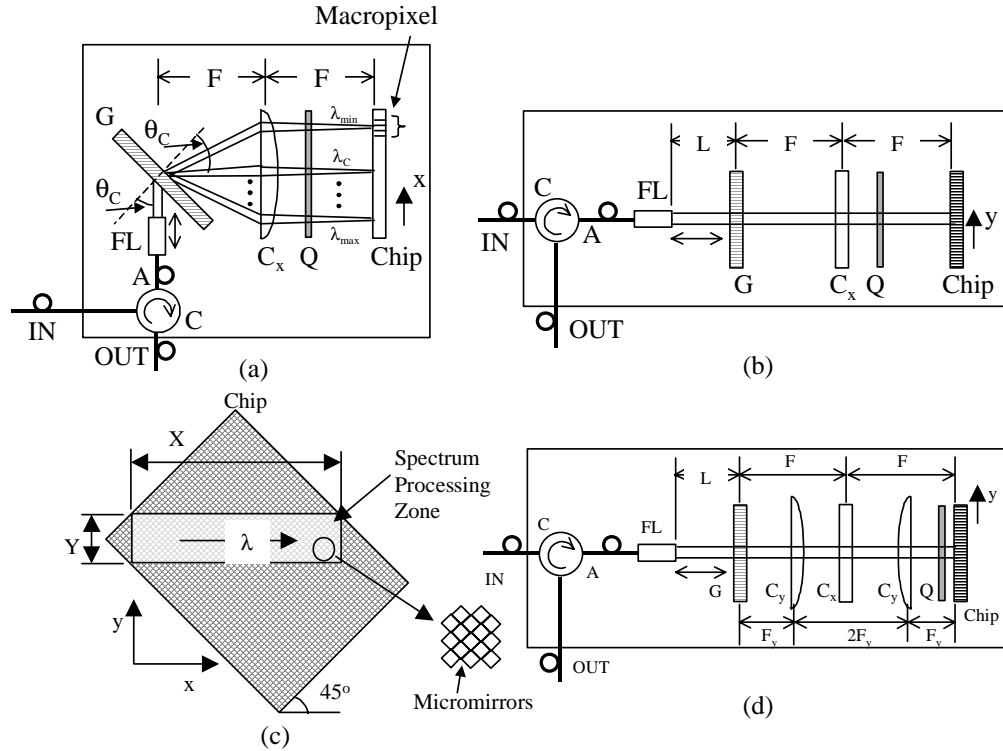


Fig. 1. (a) Top and (b) side views of the designed and demonstrated broadband equalizer using the proposed macro-pixel approach. (c) shows the orientation of the utilized DMDTM macro-pixel chip containing many micromirrors. Each micromirror is a square of side d in length. (d) shows a low coupling loss design for the equalizer via the use of a pair of cylinders to implement imaging between G and the Chip along the y -direction.

$$\theta_{\max} = \sin^{-1}[(\lambda_{\max} / l) - \sin \theta_c] \text{ and } \theta_{\min} = \sin^{-1}[(\lambda_{\min} / l) - \sin \theta_c] , \quad (1)$$

where $\lambda_{\max} - \lambda_{\min}$ is the designed spectral bandwidth of the processor with λ_{\max} and λ_{\min} the maximum and minimum processor input/output wavelengths, respectively. This angularly dispersed light from the grating passes through a focal length F cylindrical lens C_x with focusing power along the x -direction indicated in Fig. 1. The cylinder acts to collimate the angularly dispersed light from the grating so as to create a near rectangular X by Y lengths spectral processing zone at the back focal plane of C_x . A macro-pixel chip such as a tilt-mode digital micromirror device (DMDTM) shown in Fig. 1(c) is placed at this spectral processing plane with an X times Y actively controlled micromirror total area. Hence the lens C_x is located at a distance F from the chip and the grating. Because a cylindrical lens is used, the Gaussian beam in the y -direction continues to expand through free space propagation to reach a height Y at the chip plane. Given that the Gaussian beam waist radius w_i is at the grating location from where the beam starts expanding and the Gaussian beam expands for a $2F$ distance, the $1/e^2$ Gaussian beam radius w_y beam at the chip plane can be written as $w_y^2 = w_i^2 [1 + (2\lambda F / \pi w_i^2)^2]$. Since $\approx 95\%$ of the Gaussian beam energy lies with the $1/e^2$ Gaussian beam diameter $2w_y$, the optical design goal is to have $Y \geq 2w_y$ to get maximum dynamic range for attenuation control. In the orthogonal x -direction, the spectral spread at the chip plane is given via geometry as $2F \tan(\Delta\theta)$, implying that the active length X along the wavelength spread direction should satisfy the relation $X \geq 2F \tan(\Delta\theta)$ for full broadband processor design. Note that a fixed polarization rotation plate Q is placed between the lens

and the two dimensional pixelated micromirror chip. Q can be a 45 degree power Faraday rotator or a quarter waveplate (QWP). Q acts to reduce polarization dependent loss (PDL) in the equalizer due to the PDL from the grating. Because of the double-pass configuration and orthogonal state polarization flipping introduced via Q and the mirror chip, diffractions for the two orthogonal linear polarizations evens out leading to a reduced PDL from the grating. Note that the grating is naturally a polarization sensitive device due to its one dimensional grating structure; hence the use of Q can be highly beneficial. If Q is a Faraday rotator, an added benefit over broad wavelengths is that all birefringence effects between the circulator first exit port labeled “A” and the Faraday rotator can be cancelled out as shown in earlier work [15]. This in-turn can help in reducing polarization dependent dispersion (PMD) in the equalizer. Attenuation control across the wavelength band is achieved by controlling the digital tilt states of the many micromirrors that populate the spectral processing zone. In one digital state of the micromirror, light is retro-reflected back along its original path so it exits via the output port of the circular. In the other digital tilt state of a micromirror, light no longer retroreflects and hence is not directed to enter the fiber lens, thus creating optical attenuation. Because the micromirror size is small (e.g., 13.8 μm square), thousands of micromirrors fill the entire spectral processing zone creating a high resolution wavelength and power control zone that particularly helps in calibrating the module for variations in performance across the band. Moreover, since these micromirrors can be digital in operation, the equalizer becomes highly repeatable in operation. Note that the spectral processing plane diffraction limited $1/e^2$ Gaussian beam radius w_x for any grating resolvable wavelength λ is given by $w_x = (\lambda F) / (\pi w_i)$. For proper processor design so as to provide power control to the diffraction limited wavelength, the pixel size in the x-direction $d / \cos(45^\circ)$ should be less than or equal to $2w_x$. Here d is the square pixel side, and as seen in Fig. 1(c), a 45 degree angle projection is taken into consideration as the chip is oriented at this angle with respect to the wavelength or λ axis of the processor. Another important design criteria is the wavelength resolving power of the grating $\Delta\lambda$ as it sets the basic lower limit to the spectral resolution of the processor, assuming that other components (e.g., DMDTM pixel size) can spatially resolve this beam change. Using the Rayleigh criteria, $\Delta\lambda = [(l \lambda \cos \theta_c) / (2 w_i)]$, where the optically exposed grating diameter is given by $(2 w_i) / \cos \theta_c$. This $\Delta\lambda$ centered at λ leads to an angular spread in the beam given by $\delta\theta = \theta_1 - \theta_2$, where using Eq. (1) [16],

$$\theta_1 = \sin^{-1}[\{(\lambda + 0.5 \Delta\lambda) / l\} - \sin \theta_c] - \theta_c \text{ and } \theta_2 = \sin^{-1}[\{(\lambda - 0.5 \Delta\lambda) / l\} - \sin \theta_c] - \theta_c. \quad (2)$$

Considering the spatial Fourier transforming property of the cylindrical lens, the two spectrally resolved wavelengths $\lambda + 0.5 \Delta\lambda$ and $\lambda - 0.5 \Delta\lambda$ are separated by a distance approximately given by $\Delta x \sim F \{ \tan \theta_1 - \tan \theta_2 \}$. For appropriate processor design, the diffraction limited spot size for a given λ should satisfy $\Delta x \sim 2w_x$. In effect, the spatial blur spot $2w_x$ of each of the two spectrally resolved adjacent wavelengths should closely match the spatial pitch Δx between the two wavelengths to implement high spectral resolution and maximum channel count spectral processing. The next section describes how the mentioned design requirements are met to enable a powerful processor.

3. Experiments

The processor in Fig. 1 is built in the laboratory using a Texas Instruments (TI) DMDTM chip that is specifically designed for infrared C-band (1530-1565 nm) operations that matches our equalizer design where $\lambda_{\text{max}} = 1565$ nm and $\lambda_{\text{min}} = 1530$ nm. Compared to the visible band display TI DMDTM chip with bistable micromirrors with $\pm 10^\circ$ tilt angles, the present infrared chip with 786,432 mirrors is designed with $d=13.8$ μm square micromirrors operating in a bistable $\pm 9.2^\circ$ tilt angle, thus creating a high diffraction efficiency blazed grating condition.

The specified chip PDL is <0.02 dB with an individual 15 μs micromirror switching speed and a 1 ms total chip setting time through a high speed serial computer interface. The chip optical loss is measured at 1.9 dB and includes diffraction loss, pixel fill factor loss, aluminum mirror reflectivity, and hermetic seal window Fresnel loss. The specified circulator C 3-port pass loss is 1.37 dB with a PDL of 0.05 dB. The fiber lens FL has a minimum beam waist $w_i = 0.5$ mm and is placed a distance $L = 18$ cm from the grating G that has a measured 93 % diffraction efficiency (or 7% loss or 0.31 dB loss). The measured grating PDL is 0.3 dB where the grating spatial frequency is 940 lines/mm. The chosen incidence Bragg angle for the grating is $\theta_c = 46.76^\circ$ for a $\lambda_c = 1550$ nm. Using values for λ_{max} and λ_{min} , $2\Delta\theta = \theta_{\text{max}} - \theta_{\text{min}} = 2.74^\circ$. This in turn for focal length used of $F = 20$ cm gives an optically active spectral processing plane X dimension of 9.57 mm which meets our design as the X dimension on the chip that has actively programmed micromirrors is 10.92mm. The maximum diffraction limited spot size diameter $2w_x$ along the wavelength direction occurs for λ_{max} and is calculated to be 400 μm . The DMDTM pixel resolution along the x-direction is calculated to be $d/\cos(45) = 19.5$ μm which is less than the spot size resolution as required for appropriate design. The grating spectral resolution is calculated at λ_{max} to be $\Delta\lambda = 1.14$ nm which gives a Rayleigh criteria spectral blur spot pitch at λ_{max} to be $\Delta x = 320$ μm . Hence note that Δx and the $1/e^2$ Gaussian beam spot size diffraction limited diameter $2w_x$ are relatively close, as desired for design. Using custom optical components, this design can be further optimized. For the orthogonal spectral plane dimension of y, the $1/e^2$ maximum Gaussian beam diameter $2w_y$ for λ_{max} at the chip plane along the y-direction is calculated to be $2w_y = 1.08$ mm, which is also designed correctly to be less than $Y = 4.05$ mm on the actively controlled chip. Without the QWP used as Q, the equalizer PDL stays less than 0.38 dB. With the QWP inserted with its optical axis at 45° to x or y-direction, the maximum PDL is a much lower 0.1 dB. The average optical insertion loss of the equalizer is measured to be 5.2 dB. This is broken down as 1.9 dB for DMDTM effects, 1.37 dB for circulator, 0.62 dB for Grating two way loss, and 1.31 dB for free space-to-fiber coupling loss. This free space coupling loss is consistent with the loss expected from theory for a $2L + 4F = 116$ cm propagation distance when using a self-imaging type fiber lens with a 36 cm self-imaging distance [17]. Note that in the demonstrated design, the beam continues to expand in the y-direction even after reflection from the chip, adding to the total free space coupling loss. One solution proposed is shown in Fig. 1(d) where a pair of cylindrical lenses C_y with a focal length $F_y = 0.5F$ are used to implement 1:1 imaging along y between G and the chip. This unique method preserves the required Fourier transforming along x while providing imaging along y, leading to the prevention of beam spreading along y and hence reduced coupling losses.

To test the dynamic range of the processor, a single wavelength at 1550.62 nm with a linewidth of 0.06 nm is fed to the equalizer. The DMDTM chip active spectral plane of $X = 10.92$ mm by $Y = 4.05$ mm zone containing 232,960 micromirrors is set to 9.2° for retroreflection. The DMDTM area outside this zone is set to -9.2° to enable maximum dynamic range performance. Figure 2 shows the equalizer output signals for the two extreme cases of zero attenuation setting (all micromirrors in XY zone in 9.2° state) and maximum attenuation setting (all micromirrors in XY zone in -9.2° state), indicating a measured 34.24 dB attenuation dynamic range. In order to achieve this dynamic range, the active micromirror zone with -9.2° state measured 400 μm in x-direction and $Y = 4.05$ mm. This zone in turn contained 8,528 micromirrors, giving an averaged attenuation control resolution of 0.004 dB per micromirror or a better than 13 bit control resolution. Note that the designed $1/e^2$ Gaussian beam diameter at 1550.62 nm is calculated to be $2w_x = 395$ μm , which is close to the experimental 400 μm width used to provide maximum single wavelength attenuation. Hence, by controlling the micromirrors in the active zone and with appropriate equalizer calibration as the optical power is not uniformly distributed, a powerful all-digital operation equalizer is realized.

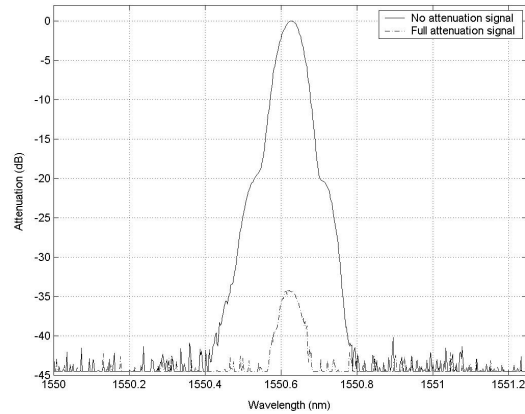


Fig. 2. Spectrum plot showing the measured 34.24 dB attenuation dynamic range of the equalizer. Solid curve showing the unattenuated 1550.62 nm input signal and the dashed curve is the maximum attenuated signal.

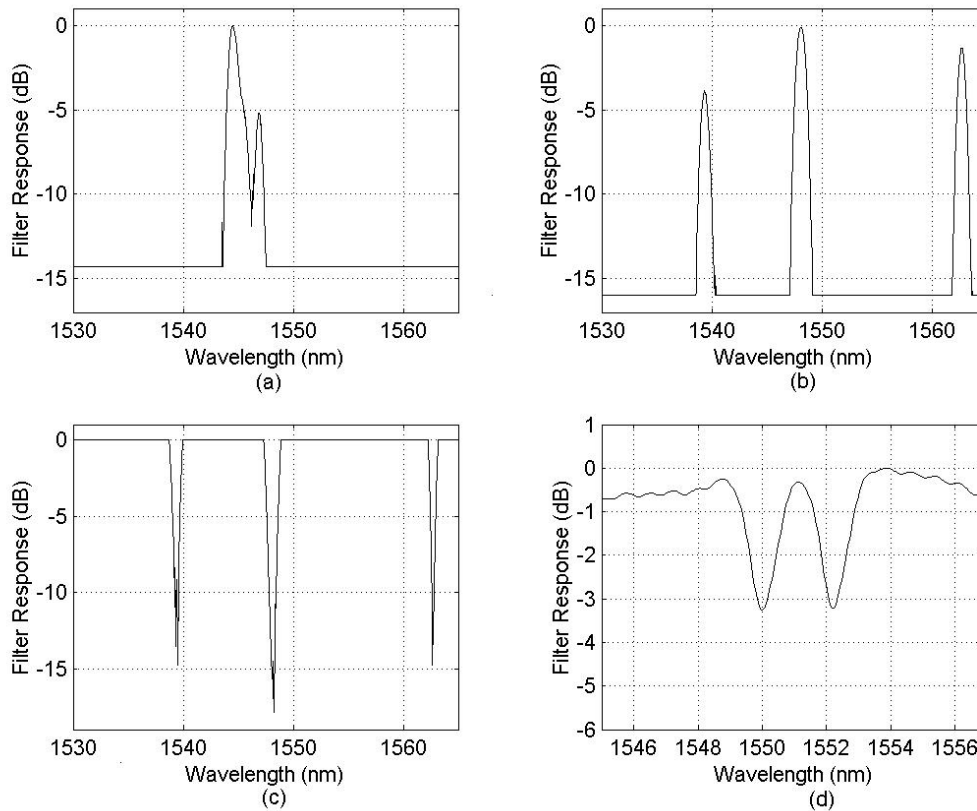


Fig. 3. Spectrum plot showing the capability of the equalizer to generate (a) generalized optical spectrum, (b) different independently controlled passbands, (c) different independently controlled notch bands. (d) The equalizer measured 2.24 nm 3 dB spectral resolution.

Figure 3(a) shows the demonstrated equalizer programmed to operate as a filter with three selective passbands, each with a particular gain weighting. These three passbands located at 1539.35 nm, 1548.10 nm, and 1562.70 nm were set by turning their respective spectral band zones on the DMD™ to 9.2° state. For these broadband tests, the equalizer is fed with light from a broadband superluminescent laser diode (SLD) and plots are normalized by

subtracting the equalizer broadband source spectrum from the equalizer processed spectrum. The capability of having independently selective passbands can be useful in applications such as on-demand WDM data transmission. Note that all optical spectrum analyzer (OSA) data is taken across the desired 1530 nm to 1565 nm band showing the broadband response of the demonstrated equalizer. As shown in Fig. 3(b), any arbitrary filter function can also be generated via the proposed equalizer by controlling the micromirror states in the DMD™ spectral processing zone. This is particularly useful when spectrum shaping is desired for enhanced signal processing capabilities. Figure 3(c) shows the demonstrated equalizer programmed to operate as a multi-notch filter with three selective notches, each with an assigned notch depth. The three notches are located at 1539.35 nm, 1548.10 nm, and 1562.70 nm and were set by turning their respective spectral band zones on the DMD™ to -9.2° state. Hence, the equalizer acts as a wavelength blocker useful in applications such as WDM communications and noise reduction in laser systems. To test the wavelength resolution of the demonstrated equalizer, two adjacent wavelengths are simultaneously attenuated by 3-dB to provide a measurement for a 3-dB wavelength resolution. Specifically, the broadband laser feeds the equalizer with all micromirrors set at 9.2° for full retroreflection of power. Next, micromirror columns centered at a chosen wavelength of 1550.02 nm are gradually turned to the alternate -9.2° state until the central notch reaches a 3 dB attenuation. Next, another central column is chosen and then gradually activated to the -9.2° state until this second independent central notch reaches a 3 dB attenuation. The key aspect of this measurement is that the centering of the micromirror columns where activation of state change starts are located sufficiently apart to enable independent 3-dB attenuation of the two different wavelengths. Figure 3(d) shows the measured result for the case where the two adjacent wavelengths providing these 3 dB notches are measured to be 1550.02 nm and 1552.26 nm, giving a 3-dB equalizer wavelength resolution of 2.24 nm. Note that this 3-dB attenuation for each independent wavelength is achieved by setting a 97.5 μm wide (corresponds to 5 diagonal orientation micromirrors) by 4.05 mm high spectral zone to -9.2° on the DMD™ chip. Considering that the designed equalizer band is 35 nm, ≈ 15 independent 3-dB wavelength resolution bands can be processed. As mentioned earlier, the wavelength slicing capability and its control in the equalizer depend on a number of key design parameters that include the grating wavelength resolution $\Delta\lambda$ and the diffraction limited spot size diameter $2w_x$. A larger beam waist radius w_i incident on the grating will decrease $2w_x$ and $\Delta\lambda$ so that an improved independent wavelength power processing sensitivity can be achieved by the equalizer. In effect, the 3-dB wavelength resolution will improve to a lower number, e.g., 0.4 nm using a larger w_i value, leading to both a broadband and high spectral resolution equalizer.

4. Conclusion

In conclusion, for the first time, the design and demonstration of a broadband high resolution optical equalizer has been described using the earlier proposed macro-pixel approach to multi-wavelength attenuation controls. The equalizer features attenuation hardware fault-tolerance, all-digital controls for enhanced repeatability, high resolution attenuation for vital calibration across wavelengths using a sparsely active micromirror array approach, and a low loss and a low PDL. The demonstrated specifications include PDL < 0.1 dB, average insertion loss < 5.2 dB, 1530-65 nm operation, 2.24 nm 3-dB wavelength resolution, 34.24 dB attenuation dynamic range, and 1 ms processing speed. Further optimized optical components can lead to improved equalizer specifications. The designed and demonstrated optical equalizer can be useful across a number of fields including biomedical optics, optical communications, laser conditioning, test and instrumentation, and aerospace systems.